Primary standardization of ^{212}Pb activity by liquid scintillation counting

Denis E. Bergeron, Jeffrey T. Cessna, Ryan P. Fitzgerald, Lizbeth Laureano-Pérez, Leticia Pibida, and Brian E. Zimmerman

Physical Measurement Laboratory, National Institute of Standards and Technology, Gaithersburg, MD 20899, USA

Keywords
Pb-212; TDCR; anticoincidence counting; efficiency tracing; radionuclide calibrator; dose calibrator; well counter; activity calibration; decay chain

Abstract

An activity standard for ^{212}Pb in equilibrium with its progeny was realized, based on triple-to-double coincidence ratio (TDCR) liquid scintillation (LS) counting. A Monte Carlo-based approach to estimating uncertainties due to nuclear decay data (branching ratios, beta endpoint energies, γ-ray energies, and conversion coefficients for ^{212}Pb and ^{208}Tl) led to combined standard uncertainties ≤ 0.20 %. Confirmatory primary measurements were made by LS efficiency tracing with tritium and 4παβ(LS)-γ(NaI(Tl)) anticoincidence counting. The standard is discussed in relation to current approaches to ^{212}Pb activity calibration. In particular, potential biases encountered when using inappropriate radionuclide calibrator settings are discussed.

1. Introduction

For cancer therapy, the short range of alpha particles in tissue means that a good radiopharmaceutical can destroy targeted cells while sparing surrounding tissue. While ^{212}Pb decays by beta emission, it is discussed in the context of targeted alpha therapy as a promising "*in vivo* generator" of ^{212}Bi, which decays to ^{208}Pb by emission of one alpha and one beta particle (Yong and Brechbiel, 2011; Poty et al., 2018; Radchenko et al., 2021). A major appeal of this approach is that, compared to ^{212}Bi ($T_{1/2}$ = 60.54(6) min; DDEP, 2021), the longer half-life of ^{212}Pb ($T_{1/2}$ = 10.64(1) h; DDEP, 2021) means that the same administered activity results in more than ten times the dose. With various combinations of chelator and bioconjugate, ^{212}Pb has now been studied as a treatment for a broad spectrum of cancers, including prostate cancers (e.g., Tan et al., 2012; Banerjee et al., 2020), melanomas (e.g., Miao et al., 2005), pancreatic cancers (e.g., Kasten et al., 2018a), breast cancers (e.g., Kasten et al., 2018b), peritoneal metastases (e.g., Meredith et al., 2014a, 2014b), and lymphomas (e.g, Maaland et al., 2020).

Accurate dosimetry and the establishment of dose-response relationships must begin with the activity assay of the radiopharmaceutical to be administered. In the preclinical and clinical studies cited above, the administered ^{212}Pb activities were measured with radionuclide calibrators or (more commonly) NaI(Tl) well counters that have been calibrated against an assay by high-purity germanium (HPGe) γ-ray spectrometry. Researchers do not often report which γ-ray emission intensities (I_γ) they have adopted for their activity assay or even which set of γ rays are measured. In most cases, it seems that the adopted data are those published by the National Nuclear Data Center (NNDC, 2021) and for ^{212}Pb these are in good accord with other evaluations, such as the Decay Data Evaluation Project (DDEP, 2021). Khan and DeWerd (2021) recently evaluated the GEANT4 package (Agostinelli et al., 2003) for targeted alpha therapy dosimetry, giving particular attention to the impact of small discrepancies in evaluated decay datasets. They found excellent accord between the databases for ^{212}Pb, but they only considered alpha decays, ignoring for their purposes a significant portion of the ^{212}Pb decay chain. In another recent study, Frelin-Labalme et al. (2020) point out the importance of an accurate assay of administered activity in their dosimetry calculations based on biodistribution studies with a Na(I)Tl counter. This type of biodistribution study is more typically discussed in relative terms.

As radiopharmaceuticals for targeted alpha therapy transition from preclinical to clinical studies, the need for standardized activity assays grows. We recently described the development of a primary activity standard for ^{224}Ra in equilibrium with its progeny, including ^{212}Pb (Napoli et al., 2020a). Here, we discuss the activity standard for ^{212}Pb separated from its progenitors and allowed to equilibrate with its progeny. We present an improved handling of uncertainties from nuclear decay data. We also expand upon the potential measurement biases, pointed out in previous works (Napoli et al., 2020b; Bergeron et al., 2022), that can arise for radionuclide calibrator assays of ^{212}Pb activity using inappropriate calibration settings.

2. Materials and Methods

2.1. Nuclear decay data

Consistent with common practice in the radionuclide metrology community (Bergeron et al., 2022), DDEP data for ^{212}Pb and its progeny were adopted in the analyses for the standard (Bé et al., 2004; Bé et al., 2014; DDEP, 2021). A newer NNDC evaluation (Martin, 2007; Auranen and McCutchan, 2020; NNDC, 2021) includes a recent precise ^{212}Pb half-life measurement from

Kossert (2017). The dates of these evaluations and the resulting equilibrium coefficients are summarized in Table 1. Figure 1 illustrates the decay chain. The data reported herein were analyzed using both data sets in order to assure that discrepancies did not significantly bias the final results; most differences between the two evaluations had no significant impact on primary activity measurements. The choice of ^{212}Pb half-life, however, can impact the activity and its uncertainty. Decay corrections calculated with the two half-lives diverge by > 0.1 % in just nine hours, prompting us to design experiments in which all decay corrections were made for intervals < 4 h. By collecting data for the primary standardization in 8 h time windows centered on the reference time (hereafter, "T_8" refers to the time window from (t_{ref} – 4 h) to (t_{ref} + 4 h)), the uncertainty due to decay corrections was minimized.

2.2. Source preparation

Experiments were performed with two shipments of ^{228}Th-produced ^{212}Pb from Orano Med (Plano, TX).[1] The ammonium acetate solution was diluted with concentrated HCl to achieve an initial volume of 1 mL. Both experiments followed the same general scheme. Experiment 1 (E1) was performed in July 2021; Experiment 2 (E2) was performed in November 2021 and used a higher starting activity. The solution composition was consistent with previous NIST work with ^{224}Ra (Napoli et al., 2020a), which included a careful validation of gravimetric links and loss-free solution transfers.

The dilution scheme adopted for both experiments can be found in the Online Supplement (Figure S1). Dilutions were carried out with 1.1 mol/L HCl (stock solution prepared from Taylor Scientific (St. Louis, MO) A.C.S. Grade). The first dilution of the incoming ^{212}Pb solution brought the HCl concentration to approximately 1.6 mol/L; after the second dilution, the HCl concentration was approximately 1.1 mol/L. In both experiments, sources were prepared gravimetrically using the aspirating pycnometer method. When practicable, the mass difference of the pycnometer before and after dispensing (dispensed mass) and the mass difference of the container before and after receiving the dispensed material (received mass) were measured. The gravimetric dilution factors were confirmed radiometrically via γ-ray spectrometry and/or ionization chamber measurements; in all cases, dilution factors agreed to within uncertainties.

All liquid scintillation (LS) sources were prepared with Ultima Gold AB (PerkinElmer, Waltham, MA) with nominal aqueous fractions of 6 % (by mass). For efficiency tracing, a series of nitromethane-quenched ^{212}Pb sources were prepared with compositions matched to a series of ^{3}H sources as prescribed by Zimmerman and Collé (1997). Distilled water was added to the ^{212}Pb sources to match the tritiated water in the ^{3}H series, while 1.1 mol/L HCl was added to the ^{3}H sources to match the ^{212}Pb series. Since Kossert reported ^{212}Pb solution instabilities when using glass scintillation vials (Kossert, 2017), all LS sources were prepared in polyethylene scintillation vials except for sources for anticoincidence counting, which were prepared in glass hemispheres. No signs of cocktail instability manifested in the data.

[1] Certain commercial equipment, instruments, or materials are identified in this Report to foster understanding. Such identification does not imply recommendation by the National Institute of Standards and Technology, nor does it imply that the materials or equipment identified are necessarily the best available for the purpose.

In both experiments, γ-ray spectrometry measurements with calibrated high-purity germanium (HPGe) detectors were carried out to look for photon-emitting impurities. No significant photon-emitting impurities were found.

2.3. Primary methods

The primary activity standardization was achieved with three liquid scintillation-based methods: triple-to-double coincidence ratio (TDCR) counting, CIEMAT/NIST efficiency tracing (CNET) with ^{3}H, and live-timed 4παβ(LS)-γ(NaI) anticoincidence counting (LTAC). The recent review by Bergeron et al. discusses in detail some of the special considerations that arise in activity standardizations of decay chain radionuclides like ^{212}Pb (Bergeron et al., 2022). Data used for the standardization were acquired after ^{212}Pb had reached equilibrium with its progeny so that decay correction to a common reference time was achieved using the $T_{1/2}$ for ^{212}Pb (Table 1). As mentioned above, the uncertainty due to decay correction was minimized by using only data acquired in T_8 for the standardization.

Equilibrium (> 99.999 %) between ^{212}Pb and its progeny occurs ≈ 12 h after separation. For both experiments, the incoming solution was received several days after separation, with measurements commencing at least one day after receipt. So, all measurements were for solutions in equilibrium and no period of progeny ingrowth was observed experimentally.

For all methods, it was assumed that the short-lived ($T_{1/2}$ ≈ 300 ns) ^{212}Po is detected with its ^{212}Bi parent, giving ≈ 100 % LS efficiency for ^{212}Po + ^{212}Bi. This is consistent with our previous treatment of the same pair in the decay of ^{224}Ra (Napoli et al., 2020a) and is discussed with several examples in (Bergeron et al., 2022).

2.3.1. Triple-to-double coincidence ratio (TDCR) counting

Sources for TDCR counting were prepared in 22 mL polyethylene scintillation vials. Efficiency variation was achieved by applying gray filters. Efficiency calculations for the β-decaying progeny of ^{212}Pb were carried out with the MICELLE2 code (Kossert and Grau Carles, 2010) using the relevant DDEP data; the LS spectra generated by MICELLE2 were compared to the BetaShape output and the results of Geant4 simulations and found to be consistent. Efficiencies for α decays were assumed to be 100 % (Cassette, 2002; Kossert et al., 2009; Fitzgerald and Forney, 2011). Simplified decay schemes were used with branch normalizations as described in (Napoli et al., 2020a). Branch normalizations based on the NNDC decay data were also considered.

As mentioned above, the simplified decay scheme assumes that ^{212}Po detected with its ^{212}Bi parent with ≈ 100 % efficiency for ^{212}Po+^{212}Bi; a 0.08 % correction is applied to the logical sum of doubles (LSD) rate to account for the rare instances when a ^{212}Bi decay is missed in one photomultiplier tube (PMT) but the ^{212}Po decay occurs after the coincidence resolving time but within the dead time. This correction assumes the ^{212}Po LS efficiency adopted in (Napoli et al., 2020a), $\varepsilon_{\text{Po-212}} > 0.995$, and a conservative uncertainty of 100 % of the correction is propagated.

Measurements were performed on a home-built three PMT system (Zimmerman et al., 2004) and data were acquired with a field programmable gate array (FPGA)-based system based on and validated against a MAC3 (Bouchard and Cassette, 2000) unit. An extending deadtime of 50 μs was applied. Application of gray filters achieved a triple-to-double coincidence ratio (R) range of

0.971 to 0.990, and corresponding to a logical sum of doubles counting efficiency (ε_D) range of (2.43 to 2.48) counts per decay, according to the MICELLE2 model. As expected for such a high-efficiency radionuclide, the model is very good; no trending with efficiency is seen in the calculated activities (Figure 2).

Corrections for accidental coincidences in the blanks and counting sources were implemented in the manner described by Dutsov et al. (2020), resulting in modest corrections to the counting data (< 0.05 %), but reducing the uncertainty due to the background by more than two orders of magnitude.

2.3.2. CIEMAT-NIST Efficiency Tracing (CNET)

Sources for CNET were prepared in 22 mL polyethylene scintillation vials. Efficiency variation was achieved via chemical quenching with nitromethane and matched tritium and blank sources were also prepared. Efficiency calculations for the β-decaying daughters of ^{212}Pb were carried out with the same MICELLE2 code and inputs used for TDCR. Input data for ^{3}H were taken from DDEP (Bé et al., 2006; DDEP, 2021).

Measurements were carried out on two commercial LS counters, a Beckman Coulter LS6500 (Beckman Coulter, Fullerton, CA, USA) and a Packard Tri-Carb 4910 (PerkinElmer, Waltham, MA, USA), with consistent results. Here again, the efficiency model provides an excellent representation of the experimental data, with no observed trending of the calculated activities with quenching (Figure 3).

2.3.3. Live-timed Anticoincidence Couting (LTAC)

Live-timed 4πβ-γ anticoincidence counting (LTAC) was performed using the NIST system consisting of a single-PMT LS detector and a NaI(Tl) well-type detector (Lucas, 1998; Fitzgerald and Schultz, 2008). Two data acquisition systems were used: a digital system using a CAEN DT5724 (Villareggio, Italy) desktop digitizer with trapezoidal filtering and an analog system using constant-fraction discriminators and a live-timing apparatus. Both systems use imposed extending dead-times of 50 μs with the γ channel delayed by 1.25 μs.

Two LS sources were prepared with initial activities of about 790 Bq and 1400 Bq. Each source was measured 3 times and a blank was measured twice, all during T_8. Then the higher activity source was measured continuously in the CAEN system for 1.5 d to check for long-lived impurities.

The LTAC analysis systems were set using 3 NaI(Tl) gates to monitor LS efficiency for three radionuclides in the ^{212}Pb chain; ^{212}Pb, ^{212}Bi, and ^{208}Tl. Spectra for the entire chain were simulated in Geant4 (Agostinelli et al., 2003) and used to determine gate settings (Figure 4) as described previously (Fitzgerald, 2016; Bergeron and Fitzgerald, 2018). LS efficiency is varied by changing the lower-level discriminator on the LS channel.

A linear fit of the count rate as a function of detection inefficiency (Y) was found in Geant4 and in the experimental data for a weighted combined inefficiency, $Y_{\text{eff}} = 0.20 \cdot Y_1 + 0.41 \cdot Y_2 + 0.39 \cdot Y_3$ (Figure 5). The extrapolation intercept was insensitive to the choices of gates, especially of gate 2, as the LS efficiency is very high for ^{212}Bi which decays either by alpha decay, or by beta decay

with the ensuing ^{212}Po alpha decay occurring within the LTAC dead time. The shape of the fit residuals matched well between the simulated and experimental data (Figure 5). As the Geant4 extrapolation using the same gates gave the correct intercept, no correction was made.

The ^{212}Pb Bateman equations were solved, including the ^{212}Po summing effect, such that the expected R_{LS} intercept, relative to the ^{212}Pb activity, is 2.5036(9) s^{-1} Bq^{-1} where the stated uncertainty is from the propagation of the DDEP decay data (Table 1) through the Bateman equations.

2.4. Ionization chamber calibration

In each experiment, several 5 mL flame-sealed ampoules (type NIST-1; Collé, 2019) were measured on reentrant ionization chambers (ICs) to establish calibration factors that will be used for subsequent calibrations of ^{212}Pb at NIST.

In the NIST automated ionization chamber (AutoIC; Fitzgerald 2010), measurements of ^{212}Pb ampoules were bracketed by measurements of a ^{226}Ra reference source (RRS). The AutoIC calibration factor (K-value) is expressed as a function of the ratio of responses measured for ^{212}Pb and the RRS. The experimental K-value was compared to a theoretical estimate based on the AutoIC response curve and input decay data. Four ampoules (see Figure S1) were measured on the AutoIC to confirm solution homogeneity before being delivered for measurement on other instruments.

The Vinten 671 ionization chamber (VIC; Woods et al., 1983) at NIST is related to sister chambers at other national metrology institutes, including the National Physical Laboratory (NPL) in Teddington, allowing for indirect comparison of activity standards (see, e.g., Bergeron and Cessna, 2018). Calibration coefficients for the VIC (K_{VIC}) are expressed directly as a function of current with units pA/MBq. RRS measurements are performed routinely (at least daily during a calibration campaign) to monitor the performance of the VIC and assure response constancy over time.

Ampoules were also measured on Capintec (Florham Park, NJ) radionuclide calibrators at several calibration settings ("dial settings") to determine which setting should give the NIST-determined activity and to evaluate biases at settings that have been suggested or recommended by others.

2.5. NaI(Tl) well counters

In each experiment, three glass scintillation vials were prepared with 10 mL of 1.1 mol/L HCl and approximately 1.5 kBq, 2.5 kBq, and 3.0 kBq of ^{212}Pb at the reference time. These sources were measured repeatedly on a Wizard 2480 (PerkinElmer, Waltham, MA) and on a Hidex AMG (Turku, Finland). Data acquired before and after T_8 will be considered in a new determination of the ^{212}Pb half-life, but are not discussed here. On both instruments, count data were acquired in a 60 keV to 110 keV window, as described by Napoli et al. (2020b) and with an "open" window.

2.6. HPGe measurements

In each experiment, ampoules were measured on high-purity germanium (HPGe) detectors to check for photon-emitting radionuclidic impurities, confirm dilution factors, and estimate solution activities based on γ-ray emission intensities. Ultimately, these data will be used in conjunction with the primary activity measurements to derive new absolute γ-ray emission intensities.

3. Results

3.1. Impurity analyses

Ampoules were measured on calibrated high-purity germanium (HPGe) detectors over the course of about one month to look for short- and long-lived photon-emitting impurities. The detection limits decreased as the ^{212}Pb decayed. Early measurements of a source containing approximately 425 kBq of ^{212}Pb in 5 mL of solution in a 5 mL ampoule and mounted 20 cm from the detector found no impurities within the following photon emission rates:

30 keV < E < 55 keV	105 s^{-1}
60 keV < E < 90 keV	170 s^{-1}
95 keV < E < 220 keV	96 s^{-1}
225 keV < E < 255 keV	197 s^{-1}
260 keV < E < 490 keV	91 s^{-1}
500 keV < E < 520 keV	147 s^{-1}
530 keV < E < 560 keV	80 s^{-1}
570 keV < E < 600 keV	230 s^{-1}
610 keV < E < 2000 keV	89 s^{-1}

Thirty days later, when the ^{212}Pb was no longer detectable, measurements were performed at a closer distance and on a different HPGe detector. No impurities were detected within the following photon emission rates:

30 keV < E < 40 keV	4.4 s^{-1}
50 keV < E < 65 keV	0.46 s^{-1}
70 keV < E < 85 keV	0.27 s^{-1}
90 keV < E < 235 keV	0.24 s^{-1}
235 keV < E < 240 keV	0.26 s^{-1}
245 keV < E < 2000 keV	0.26 s^{-1}
2000 keV < E < 2600 keV	0.22 s^{-1}
2610 keV < E < 2620 keV	0.52 s^{-1}

In addition to photon-emitting impurities, LS measurements were acquired with the LTAC and TDCR systems over several days to confirm that no pure α- or β- emitting impurities were present.

3.2. Triple-to-double Coincidence Ratio (TDCR) Counting

As for ^{224}Ra (Napoli et al., 2020a), the TDCR results were adopted for the primary activity standard for ^{212}Pb. Table 2 shows the detailed uncertainty budgets for E1 and E2. In E1, the difference between the activities determined using the DDEP and NNDC data was 0.0037 % for T_8; expanding the time window to include data collected over 40 h increased the difference to 0.037 %. In E2, the difference for T_8 was 0.0049 % and for the 40 h window it increased to 0.063 %. While the smaller uncertainty on the NNDC-recommended half-life results in a slightly smaller uncertainty component for the decay correction, in both experiments, this is offset by apparently slightly poorer counting statistics when using the NNDC data. In fact, this is not due to counting statistics; the decay-corrected massic activities trend very slightly with time, indicating that the

data are in better agreement with the DDEP half-life. Considering only T_8 data, these differences and trends are exceedingly small (*vide supra*).

In both experiments, the largest contributors to the combined standard uncertainty were the nuclear decay data and the counting statistics. For both TDCR and CNET, the uncertainty due to the nuclear decay data was estimated using a Monte Carlo approach, resulting in a much smaller contribution than was achieved using a more conservative approach in the standardization of ^{224}Ra (Napoli et al., 2020a). A script was written in LabVIEW 2021 (National Instruments, Austin, TX) to revise the MICELLE2 input files by sampling from gaussian distributions defined by DDEP adopted values and uncertainties for the branching ratios, beta endpoint energies, γ-ray energies, and conversion coefficients for ^{212}Pb and ^{208}Tl. For each nuclide, the script was run for 25000 iterations (with 5000 MICELLE2 decays per branch in each iteration) and the outputs compiled into efficiency distributions. The distributions were consistent with the "true" MICELLE2 runs (no variation of input data, 50000 decays per branch). To estimate the uncertainty on the efficiencies, a representative TDCR (or, for CNET, tritium efficiency) was selected and the standard deviation on the corresponding efficiencies was calculated. For example, for a tritium efficiency of 0.3047 counts per decay, the average (N = 22100) ^{212}Pb efficiency was 0.9703 counts per decay with a relative standard deviation of 0.13 %. This propagates to a 0.054 % relative uncertainty on the full-chain efficiency of 2.47 counts per ^{212}Pb decay.

3.3. Efficiency Tracing

The CNET results were considered confirmatory. Table 3 shows the detailed uncertainty budget for E1 and E2, based on the T_8 data. The uncertainty due to nuclear decay data includes the Monte Carlo propagation of uncertainties for the branching ratios, beta endpoint energies, γ-ray energies, and conversion coefficients for ^{212}Pb and ^{208}Tl described in Section 3.2. In E1, the difference between the activities determined using the DDEP and NNDC data was 0.011 % for T_8; in E2, the difference was 0.009 %.

3.4. Anticoincidence Counting

The LTAC results were considered confirmatory. In E1, LTAC was not successful due to a technical problem that was not recognized before T_8 had elapsed. The problem was fixed for E2 and Table 4 shows the detailed uncertainty budget. The largest contributions to the uncertainty were from the extrapolation (assessed by trying multiple weights and a quadratic fit, and through Monte Carlo modelling) and measurement repeatability (standard deviation of the distribution for the 6 measurements). The half-life uncertainty was < 0.01 %. The difference between the activities determined using the DDEP and NNDC decay data was 0.0015 % for T_8.

3.5. Links and calibrations

3.5.1. Between-method and -experiment agreement

The massic activities of ^{212}Pb determined by TDCR, CNET and LTAC were in good agreement in both experiments. In E1, the ratio of the CNET- and TDCR-determined activities was A_{CNET}/A_{TDCR} = 0.9980(22), where the stated uncertainty is from CNET only. In E2, the ratio was A_{CNET}/A_{TDCR} = 1.0005(28). In E2, the LTAC-determined activity, too, was consistent with TDCR, giving A_{LTAC}/A_{TDCR} = 1.0011(30) where the stated uncertainty is from LTAC only.

The good between-method agreement was accompanied by good between-experiment agreement (see also Section 3.5.2). The VIC calibration factors (K_{VIC}) determined in E1 and E2 from the TDCR activity with the DDEP decay data gave a ratio of K_{E1}/K_{E2} = 0.9965(32), where the stated uncertainty is taken only from E2. Between-experiment agreement was further confirmed using HPGe γ-ray spectrometry with the 2.6 MeV γ ray from ^{208}Tl. Here, the activity ratio A_{E1}/A_{E2} = 0.997(6), where the stated uncertainty is from only the more precise E2 measurement.

3.5.2. Ionization chambers/radionuclide calibrators

AutoIC K values for radium reference source RRS50 were determined in both E1 and E2 and compared to a theoretical K value. Results are shown in Table 5, in which the offset of the measurement time from the reference time is also indicated. The final value for AutoIC was taken as the value from E2, measured at the reference time, as it was insensitive to the choice of half-life. The combined standard uncertainty is 0.23 %, as described in Table 6. This K value will be used for future NIST calibrations of ^{212}Pb activity. In addition, the AutoIC measurements were used as a check of solution homogeneity. The relative standard deviation on the massic AutoIC response for four ampoules (see Figure S1) was 0.024 % in E1 and 0.022 % in E2; in all instances, these values were slightly less than the relative standard deviation of the mean on repeated current measurements of a single ampoule (see Table 6).

The final adopted value for 5 mL of a 1 mol/L HCl solution of ^{212}Pb in equilibrium with its progeny in a NIST standard 5 mL flame sealed ampoule, based on the E2 results and a decay correction with the DDEP half-life, is K_{VIC} = 13.27(4) pA/MBq. Importantly, because the VIC data were collected outside of T_8, the uncertainty due to the decay correction contributes significantly to the combined standard uncertainty (Table 7). Further, the K_{VIC} determination is sensitive to the half-life used (i.e., DDEP or NNDC). A future reevaluation of the ^{212}Pb half-life may prompt a re-analysis of these data; if the NNDC value were adopted, K_{VIC} would change by -0.44 %.

Measurements were also performed on several Capintec radionuclide calibrators (representative data included in Online Supplemental Material). The calibration numbers ("dial settings") expected to return the correct (according to the contemporaneous TDCR measurements) activity for each instrument were determined using the calibration curve method (Zimmerman and Cessna, 2000). Uncertainties were estimated by combining components for the uncertainty on the standard activity with the uncertainty due to the half-life corrections (< 0.15 %) and the uncertainty due to the calibration curve fit (0.05 % to 0.14 %, encompassing measurement repeatability). Table 8 gives a summary of the dial setting determinations.

As discussed by Bergeron et al. (2022), the dial settings found in the Capintec manual (Capintec Inc., 1986) were estimated for ^{212}Pb in isolation and for ^{212}Pb in equilibrium with ^{212}Bi. A pair of settings (30 and 146) is provided that should show the sum of ^{212}Pb and ^{212}Bi activities when the two nuclides are at equilibrium (the reading acquired with DS = 146 is to be multiplied by a factor of 2). Of course, if ^{212}Pb is allowed to equilibrate with ^{212}Bi, then subsequent progeny will also contribute to the instrument response.

So, these settings will not return the correct activity for ^{212}Pb in equilibrium with its progeny. Table 9 shows the bias observed when measuring a ^{212}Pb source on a Capintec CRC-15R using the settings found in the Capintec manual. In all instances, the activity reading is much higher than the true ^{212}Pb activity. This is expected since the main contributor to ionization chamber response from

^{212}Pb in equilibrium with its progeny should be ^{208}Tl, with its γ-ray emissions at 510.7 keV (I_γ = 22.5(2) %), 583.2 keV (I_γ = 85.0(3) %), and 2614.5 keV (I_γ = 99.755(4) %) (DDEP, 2021).

Considering the equilibrium coefficients and expected ionization chamber responses based on an EGSnrc model benchmarked against the one described by Townson et al. (2018), ^{208}Tl is expected to account for ≈ 80 % of the total VIC response. This proportion will be quantitatively different for the thicker-walled Capintec chambers, but the qualitative effect explains the biases shown in Table 9.

The NIST-determined calibration setting for the Capintec CRC-55tR differs slightly from the setting reported by Napoli et al. (2020b) for the same geometry (see Tables 8 & 9). At *DS* = 662, the activity reading was overestimated by ≈ 4 % (Table 9). The activity assay used by Napoli et al. to determine their setting was based on HPGe γ-ray spectrometry using the evaluated emission intensities for the 238 keV and 300 keV γ rays. They report an expanded (k = 2) uncertainty on their CRC-55tR-determined activities of 10.16 %, putting their results in accord with ours. We note that our HPGe activity measurements, based on the 238 keV γ ray (I_γ = 43.6(5) photons per 100 ^{212}Pb decays; DDEP, 2021), found $A_{\mathrm{HPGe}}/A_{\mathrm{TDCR}}$ = 0.9963(59).

Finally, because of the relatively low energy x-rays and bremsstrahlung encountered in the beta decay of ^{212}Pb and some progeny, changes in sample composition may affect the results of measurements with ionization chambers. Therefore, the results reported here should be considered valid for only the specific solution composition and containers described and for the actual chambers maintained by NIST. Users should verify the validity of reported settings on their own systems.

3.5.3. Well-type NaI(Tl) detectors

Table 10 summarizes the results of measurements on the Wizard and Hidex well-type NaI(Tl) detectors. Calibration coefficients are reported with units counts per ^{212}Pb decay (equivalent to counts per second per becquerel). In all cases, the largest contributor to the combined standard uncertainty was the uncertainty on the standard activity. Counting uncertainties, source-to-source variance, and the uncertainty on the decay correction were all minor contributors.

A Geant4 Monte Carlo model for the Wizard 2480, benchmarked with ^{18}F and successfully used to predict the response for ^{224}Ra (Napoli et al., 2020a), predicted a response in the 15 keV to 2047 keV window of 1.064 counts per ^{212}Pb decay, consistent with the measured response. The experiment-to-experiment agreement in the Wizard response was excellent.

For φ12 mm × 75 mm glass tubes in a Hidex counter, Napoli et al. (2020b) reported volume-dependent calibration coefficients ranging from 17.27 CPM/Bq to 17.77 CPM/Bq (where "CPM" refers to counts per minute) in the 60 keV to 110 keV window; this range corresponds to 0.288 counts per ^{212}Pb decay to 0.296 counts per ^{212}Pb decay.

4. Summary and Conclusions

NIST has developed a radioactivity standard for ^{212}Pb in equilibrium with its progeny. The primary activity standard is based on triple-to-double coincidence ratio (TDCR) liquid scintillation

counting, with efficiencies for beta-emitting progeny calculated using the MICELLE2 code. The standard was confirmed by CIEMAT-NIST efficiency tracing (CNET) with tritium and live-timed anticoincidence (LTAC) counting, with agreement ≤ 0.20 %. Uncertainties on LS efficiencies due to nuclear decay data uncertainties were estimated with a Monte Carlo approach, yielding a significant reduction in the combined standard uncertainty relative to what was recently estimated for ^{224}Ra.

The TDCR-based standard was consistent with the activity determined by HPGe γ-ray spectrometry using the DDEP-recommended emission intensity for the 238 keV γ ray. Theoretically predicted responses for ionization chambers and a NaI(Tl) well counter were also consistent.

The standard was transferred to several ionization chambers, including the NIST AutoIC. The K value for the AutoIC has a combined standard uncertainty of 0.23 %. Future NIST calibrations of ^{212}Pb in 1 mol/L HCl will be performed on this instrument.

Radionuclide calibrator measurements were performed, illustrating the large biases that can be expected from activity assays using inappropriate settings determined for ^{212}Pb in isolation or in equilibrium with only a subset of its progeny. The majority of preclinical and clinical studies involving ^{212}Pb appear to use activity assays based on γ-ray spectrometry. In some cases, this assay has been performed by the isotope supplier, and in others, by the end-users themselves. Often, activity calibrations by γ-ray spectrometry have been used as the basis for radionuclide calibrator and/or NaI(Tl) well counter calibrations. Given the consistency between our HPGe and TDCR assays, it is probable that properly performed γ-ray spectrometry has provided a solid basis for activity measurements preceding the development of this first primary activity standard for ^{212}Pb.

Acknowledgements
This work was supported in part by Orano Med, Plano, TX.

5. References

Agostinelli, S., Allison, J., Amako, E., et al., 2003. GEANT4 – a simulation toolkit. Nucl. Inst. Methods Phys. Res. A 506m, 250–303.

Auranen, K., McCutchan, E.A., 2020. Nuclear Data Sheets for A=212*. Nucl. Data Sheets 168, 117-267.

Banerjee, S.R., Minn, I., Kumar, V., Josefsson, A., Lisok, A., Brummet, M., Chen, J., Kiess, A.P., Baidoo, K., Brayton, C., Mease, R.C., Brechbiel, M., Sgouros, G., Hobbs, R.F., Pomper, M.G., 2020. Preclinical evaluation of $^{203/212}$Pb-labeled low-molecular-weight compounds for targeted radiopharmaceutical therapy of prostate cancer. J. Nucl. Med. 61, 80-88.

Bé, M.-M., Chisté, V., Dulieu, C., Browne, E., Chechev, V., Kuzmenko, N., Helmer, R., Nichols, A., Schönfeld, E., Dersch, R., 2004. Table of Radionuclides, vol. 2. A = 151 to 242. Monographie BIPM-5.

Bé, M.-M., Chisté, V., Dulieu, C., Browne, E., Bagin, C., Chechev, V., Kuzmenco, N., Helmer, R., Kondev, F., MacMahon, D., Lee, K.B., 2006. Table of Radionuclides, vol. 3. A = 3 to 244. Monographie BIPM-5.

Bé, M.-M., Chisté, V., Dulieu, C., Mougeot, X., Chechev, V.P., Nichols, A.L., Huang, X., Wang, B., 2013. Table of Radionuclides, vol. 7. A = 14 to 245. Monographie BIPM-5.

Bergeron, D.E., Cessna, J.T., 2018. An update on 'dose calibrator' settings for nuclides used in nuclear medicine. Nuclear Medicine Communications 39, 500-504.
Bergeron, D.E., Fitzgerald, R., 2018. Monte Carlo modelling of live-timed anticoincidence (LTAC) counting for Cu-64. Appl. Radiat. Isot. 134, 280-285.
Bergeron, D.E., Kossert, K., Collins, S.M., Fenwick, A.J., 2022. Realization and dissemination of activity standards for medically important alpha-emitting radionuclides. Appl. Radiat. Isot. 184, 110161.
Bouchard, J., Cassette, P., 2000. MAC3: an electronic module for the processing of pulses delivered by a three photomultiplier liquid scintillation counting system. Appl. Radiat. Isot. 52, 669-672.
Capintec Inc, 1986. Radionuclide Calibrator Owner's Manual, Revision E. Ramsey. Capintec Inc, NJ.
Cassette, P., 2002. Evaluation of the influence of wall effects on the liquid scintillation counting detection efficiency for the standardization of high-energy beta and alpha radionuclides. Möbius, S., Noakes, J.E., Schönhofer, F., Eds., LSC2001, Advances in Liquid Scintillation Spectrometry. Tucson: Radiocarbon, pp. 45-55.
Collé, R., 2019. Ampoules for Radioactivity Standard Reference Materials™. NISTIR 8254, https://doi.org/10.6028/NIST.IR.8254.
DDEP, accessed 2021: http://www.lnhb.fr/nuclear-data/nuclear-data-table/
Dutsov, C., Cassette, P., Sabot, B., Mitev, K., 2020. Evaluation of accidental coincidence counting rates in TDCR counting. Nucl. Instrum. Methods Phys. Res. A 977, 164292.
Fitzgerald, R., Schultz, M.K., 2008. Liquid-scintillation-based anticoincidence counting of Co-60 and Pb-210. Appl. Radiat. Isot. 66, 937-940.
Fitzgerald, R., 2010. An automated ionization chamber for secondary radioactivity standards. Appl. Radiat. Isot. 68, 1507-1509.
Fitzgerald, R., Forney, A.M., 2011. Determination of the Wall Effect for Alpha Emitters. Ph. Cassette, Editor, LSC2010. Advances in Liquid Scintillation Spectrometry. Tucson: Radiocarbon, pp. 331-339.
Fitzgerald, R., 2016. Monte Carlo based approach to the LS-NaI 4πβ-γ coincidence counting. Metrologia 52, S86-S96.
Frelin-Labalme, A.-M., Roger, T., Falzone, N., Lee, B.Q., Sibson, N.R., Vallis, K.A., Myriam, B., Samuel, V., Corroyer-Dulmont, A., 2020. Radionuclide spatial distribution and dose deposition for in vitro assessments of ^{212}Pb-alphaVCAM-1 targeted alpha therapy. Med. Phys. 47, 1317-1326.
Khan, A.U., DeWerd, L.A., 2021. Evaluation of the GEANT4 transport algorithm and radioactive decay data for alpha particle dosimetry. Appl. Radiat. Isot. 176, 109849.
Kasten, B.B., Gangrade, A., Kim, H., Fan, J., Ferrone, S., Ferrone, C.R., Zinn, K.R., Buchsbaum, D.J., 2018a. ^{212}Pb-labeled B7-H3-targeting antibody for pancreatic cancer therapy in mouse models. Nucl. Med. Biol. 58, 67-73.
Kasten, B.B., Oliver, P.G., Kim, H. Fan, J., Ferrone, S., Zinn, KR., Buchsbaum, D.J., 2018b. ^{212}Pb-labeled antibody 225.28 targeted to chondroitin sulfate proteoglycan 4 for triple-negative breast cancer therapy in mouse models. Int. J. Mol. Sci. 19, doi:10.3390/ijms19040925.
Kossert, K., Jörg, G., Nähle, O., v. Gostomoski, C.L., 2009. High precision measurement of the half-life of ^{147}Sm. Appl. Radiat. Isot. 67, 1702-1706.
Kossert, K., Grau Carles, A., 2010. Improved method for the calculation of the counting efficiency of electron-capture nuclides in liquid scintillation samples. Appl. Radiat. Isot. 68, 1482-1488.
Kossert, K., 2017. Half-life measurement of ^{212}Pb by means of a liquid scintillator-based ^{220}Rn trap. Appl. Radiat. Isot. 125, 15-17.
Lucas, L.L., 1998. Calibration of the massic activity of a solution of Tc-99. Appl. Radiat. Isot. 49, 1061-1064.
Maaland, A.F., Saidi, A., Torgue, J., Heyerdahl, H., Stallons, T.A.R., Kolstad, A., Dahle, J., 2020. Targeted alpha therapy for chronic lymphocytic leukaemia and non-Hodgkin's lymphoma with the anti-CD37 radioimmunoconjugate ^{212}Pb-NNV003. PLoS ONE 15, e0230526.
Martin, J.J., 2007. Nuclear Data Sheets for A=208*. Nucl. Data Sheets 108, 1583-1806.

Meredith, R.F., Torgue, J., Azure, M.T., Shen, S., Saddekni, S., Banaga, E., Carlise, R., Bunch, P., Yoder, D., Alvarez, R., 2014a. Pharmacokinetics and imaging of ^{212}Pb-TCMC-Trastuzumab after intraperitoneal administration in ovarian cancer patients. Cancer Biother. Radiopharm. 29, 12-17.

Meredith, R., Torgue, J., Shen, S., Fisher, D.R., Banaga, E., Bunch, P., Morgan, D., Fan, J., Straughn, Jr., J.M., 2014b. Dose escalation and dosimetry of first-in-human α radioimmunotherapy with ^{212}Pb-TCMC-trastuzumab. J. Nucl. Med. 55, 1636-1642.

Miao, Y., Hylarides, M., Fisher, DR., Shelton, T., Moore, H., Wester, D.W., Fritzberg, A.R., Winkelmann, C.T., Hoffman, T., Quinn, T.P., 2005. Melanoma therapy via peptide-targeted α-radiation. Clin. Cancer Res. 11, 5616-5621.

Napoli, E., Cessna, J.T., Fitzgerald, R., Pibida, L., Collé, R., Laureano-Pérez, L., Zimmerman, B.E., Bergeron, D.E., 2020a. Primary standardization of ^{224}Ra activity by liquid scintillation counting. Appl. Radiat. Isot. 155, 108933.

Napoli, E., Stenberg, V.Y., Juzeniene, A., Hjellum, G.E., Bruland, O.S., Larsen, R.H., 2020b. Calibration of sodium iodide detectors and reentrant ionization chambers for ^{212}Pb activity in different geometries by HPGe activity determined samples. Appl. Radiat. Isot. 166, 109362.

NNDC, accessed 2021: https://www.nndc.bnl.gov/ensdf/

Poty, S., Francesconi, L.C., McDevitt, M.R., Morris, M.J., Lewis, J.S., 2018. α-Emitters for Radiotherapy: From Basic Radiochemistry to Clinical Studies—Part 1. J. Nucl. Med. 59, 878-884.

Radchenko, V., Morgenstern, A., Jalilian, A.R., Ramogida, C.F., Cutler, C., Duchemin, C., Hoehr, C., Haddad, F., Bruchertseifer, F., Gausemel, H., Yang, H., Osso, J.A., Washiyama, K., Czerwinski, K., Leufgen, K., Pruszyński, M., Valzdorf, O., Causey, P., Schaffer, P., Perron, R., Maxim, S., Wilber, D.S., Stora, T., Li, Y., 2021. Production and Supply of α-Particle—Emitting Radionuclides for Targeted α-Therapy. J. Nucl. Med. 62, 1495-1503.

Tan, Z., Chen, P., Schneider, N., Glover, S., Cui, L, Torgue, J., Rixe, O., Spitz, H.B., Dong, Z., 2012. Significant systemic therapeutic effects of high-LET immunoradiation by ^{212}Pb-trastuzumab against prostatic tumors of androgen-independent human prostate cancer in mice. Int. J. Oncol. 40, 1881-1888.

Townson, R., Tessier, F., Galea, R., 2018. EGSnrc calculation of activity calibration factors for the Vinten ionization chamber. Appl. Radiat. Isot. 134, 100-104.

Woods, M.J., Callow, W.J., Christmas, P., 1983. The NPL radionuclide calibrator—type 271. Nucl. Med. Biol. 10, 127-132.

Yong, K., Brechbiel, M.W., 2011. Towards translation of ^{212}Pb as a clinical therapeutic; getting the lead in! Dalton Trans. 40, 6068-6076.

Zimmerman, B.E., Collé, R., 1997. Standardization of Ni-63 by 4 pi beta liquid scintillation spectrometry with H-3-standard efficiency tracing. J. Res. Natl. Inst. Stand. Technol. 102, 455-477.

Zimmerman, B.E., Cessna, J.T., 2000. Experimental determinations of commercial 'dose calibrator' settings for nuclides used in nuclear medicine. Appl. Radiat. Isot. 52, 615-619.

Zimmerman, B.E., Collé, R., Cessna, J.T., 2004. Construction and implementation of the NIST triple-to-double coincidence ratio (TDCR) spectrometer. Appl. Radiat. Isot. 60, 433-438.

Table 1 The decay data used in this Report were taken from the most recent DDEP evaluation. Equilibrium coefficients were calculated from the Bateman equations. Uncertainties on the equilibrium coefficients owe mostly to the uncertainties on the ^{212}Pb half-life and the ^{212}Bi α/β branching ratio. The DDEP evaluation indicates that 64.07(7) % of decays proceed via β^- emission to ^{212}Po and the remainder via α emission to ^{208}Tl. Data from the more recent NNDC evaluation are also shown. The NNDC evaluation indicates that 64.06(6) % of ^{212}Bi decays proceed via β^- emission and the equilibrium coefficients differ only slightly from those determined with the DDEP data.

	Nuclide	Evaluation Date	Evaluator	$T_{1/2}$	Equilibrium coefficient
DDEP	^{212}Pb	May 2010	A.L. Nichols	10.64(1) h	1
	^{212}Bi	May 2010	A.L. Nichols	60.54(6) min	1.10477(16)
	^{212}Po	May 2010	A.L. Nichols	300(2) ns	0.7078(8)
	^{208}Tl	July 2010	A.L. Nichols	3.058(6) min	0.3988(8)
NNDC	^{212}Pb	August 2020	K. Auranen and E.A. McCutchan	10.622(7) h	1
	^{212}Bi	August 2020	K. Auranen and E.A. McCutchan	60.55(6) min	1.10498(14)
	^{212}Po	August 2020	K. Auranen and E.A. McCutchan	294.3(7) ns	0.7079(7)
	^{208}Tl	June 2007	M.J. Martin	3.053(4) min	0.3990(7)

Table 2 TDCR ^{212}Pb massic activity uncertainty budget.

Uncertainty Component	*u* / %	
	E1	E2
Counting statistics (within and between insertions)	0.11	0.11
Model uncertainty (efficiency variation); estimated as the typical standard deviation on measurements of a source with (N = 3) different gray filters	0.05	0.08
Between sources; estimated as the standard deviation on the activity concentration obtained with (N = 3) LS sources	0.09	0.03
Background	2E-05	4E-05
Pb-212 half-life; propagation of the standard uncertainty on the half-life for ^{212}Pb (DDEP: 10.64(1) h)	0.002	0.005
Nuclear decay data: estimated uncertainty due to the half-lives and branching ratios of ^{212}Pb and its progeny at equilibrium predicted by the Bateman Equation (dominated by the uncertainty on the ^{212}Bi decay branching ratio); uncertainty due to beta shape and endpoint uncertainties; uncertainty due to missed coincidences in the ^{212}Bi+^{212}Po decay	0.12	0.11
Efficiency Model (quenching model); propagation of an estimated uncertainty on the Birks parameter (kB = 0.0075(15) MeV/cm)	0.03	0.03
Mass determinations	0.05	0.05
Combined standard uncertainty	**0.20**	**0.18**

Table 3 CNET ^{212}Pb massic activity uncertainty budget.

Uncertainty Component	*u* / %	
	E1	E2
Counting statistics; typical cycle-to-cycle variance (including only T_8 data), combined with run-to-run variance (including data outside T_8)	0.11	0.20
Between sources; estimated as the standard deviation on the activity concentration obtained with (N = 5) differently quenched LS sources	0.14	0.11
Between counters; estimated as half the difference between the massic activities determined with the Beckman and Packard LS counters	0.10	0.12
Background; wholly embodied in statistics		
Massic activity of ^{3}H (for uncertainty in standard of 0.54 %)	0.02	0.01
Pb-212 half-life; propagation of the standard uncertainty on the half-life for ^{212}Pb (DDEP: 10.64(1) h)	0.016	0.05
H-3 half-life (12.312(25) a; DDEP, 2021)	3E-6	1E-5
Nuclear decay data: estimated uncertainty due to the half-lives and branching ratios of ^{212}Pb and its progeny at equilibrium predicted by the Bateman Equation (dominated by the uncertainty on the ^{212}Bi decay branching ratio); uncertainty due to beta shape and endpoint uncertainties	0.07	0.07
Efficiency Model (quenching model); propagation of an estimated uncertainty on the Birks parameter (kB = 0.0075(15) MeV/cm)	0.01	0.01
Mass determinations	0.05	0.05
Combined standard uncertainty	**0.22**	**0.28**

Table 4 LTAC ^{212}Pb massic activity uncertainty budget for E2.

Uncertainty Component	u / %
Repeatability: Estimated as the standard deviation for $N = 6$ measurements (each of 3 sources measured twice). No trends with time, count rate, or between sources.	0.16
Extrapolation: Estimated as the standard deviation of intercepts from 7 extrapolations using various weights, linear and quadratic	0.22
Live-time: Estimated based on previous tests. No trends seen with count rate.	0.10
Weighing	0.05
Background	0.07
Pb-212 half-life; propagation of the standard uncertainty on the half-life for ^{212}Pb (DDEP: 10.64(1) h)	0.008
Combined standard uncertainty	**0.30**

Table 5 K value determinations for AutoIC. The value adopted for future NIST calibrations ($K_{adopted}$) is from E2, measured at the reference time and decay-corrected using the DDEP half-life. It has a relative combined standard uncertainty of 0.23 %. K values determined at other times or with the NNDC half-life are reported relative to $K_{adopted}$, with their relative combined standard uncertainties given in parentheses.

Expt.	Half-life	$(t_{meas} - t_{ref})$ / d	$K/K_{adopted}$
E1	DDEP	-1	0.9989(25)
E1	NNDC	-1	1.0015(23)
E2	DDEP	-2	0.9997(32)
E2	NNDC	-2	1.0043(26)
E2	DDEP	0	1
E2	NNDC	0	1.0001(26)
Theory	N/A	N/A	1.004(18)

Table 6 AutoIC K value uncertainty budget.

Uncertainty Component	*u* / %
TDCR activity: combined standard uncertainty	0.18
Measurement: combined standard deviations of the mean for 64 ^{212}Pb source readings, 3 radium reference source readings, and 4 background readings.	0.05
Source positioning: Standard deviation of the distribution for the massic current from 4 ampoules, measured previously	0.02
Pb-212 half-life; propagation of the standard uncertainty on the half-life for ^{212}Pb (DDEP: 10.64(1) h)	0.01
Laboratory conditions: estimated from potential bias due to different temperature and relative humidity during source and RRS measurements	0.10
Weighing, dilution	0.09
Combined standard uncertainty	**0.23**

Table 7 VIC K_{VIC} uncertainty budget.

Uncertainty Component	u / %
TDCR activity: standard combined uncertainty	0.18
Measurement: typical within and between-insertion variance for a single source with (N = 200) readings per insertion, combined with estimated between-source variance	0.02
Pb-212 half-life; propagation of the standard uncertainty on the half-life for ^{212}Pb (DDEP: 10.64(1) h)	0.24
Weighing, dilution	0.09
Combined standard uncertainty	**0.32**

Table 8 Dial settings (*DS*) determined by the calibration curve method to give the correct ^{212}Pb activity for 5 mL of a 1 mol/L HCl solution of ^{212}Pb in equilibrium with its progeny in a NIST standard 5 mL flame sealed ampoule. Uncertainties on the dial settings, in dial setting units, are given in parentheses and are expanded (k = 2) uncertainties. The resulting relative expanded uncertainty on the measured activity (U_A) is given in the last row.

	CRC-15R	CRC-35R	CRC-55tR	CRC-25PET	CRC-55tPET
DS_{TDCR}	690(4)	693(3)	688(4)	696(3)	685(3)
U_A / %	0.45	0.41	0.49	0.38	0.37

Table 9 Response to a 5 mL ampoule containing ^{212}Pb in equilibrium with its progeny measured in a Capintec CRC-15R radionuclide calibrator at several settings. The activity readings (A_{read}) are shown relative to the TDCR-determined ^{212}Pb activity (A_{TDCR}).

DS	A_{read} / A_{TDCR}	Note
101	4.20	*DS* given in manual for ^{212}Pb in isolation.
158	3.23	*DS* given in manual for ^{212}Pb in equilibrium with ^{212}Bi.
30	6.83	*DS* given in manual for sum of ^{212}Pb and ^{212}Bi activity
146	3.40	*DS* given in manual for sum of ^{212}Pb and ^{212}Bi activity (to be multiplied by 2)
571	1.18	*DS* given in manual for ^{208}Tl (to be divided by 2)
662	1.04	*DS* reported by Napoli et al. for ^{212}Pb

Table 10 Calibration coefficients based on the TDCR activity in each experiment. No data were acquired on the Hidex AMG well counter in Experiment 2.

	Wizard 2480		Hidex AMG	
	15 keV to 2047 keV	**60 keV to 110 keV**	**open**	**60 keV to 110 keV**
E1	1.068(3)	0.298(1)	0.971(3)	0.296(1)
E2	1.067(3)	0.298(1)	-	-

Figure 1 Decay chain of ^{212}Pb and progeny to stable ^{208}Pb. Relevant decay data are summarized in Table 1.

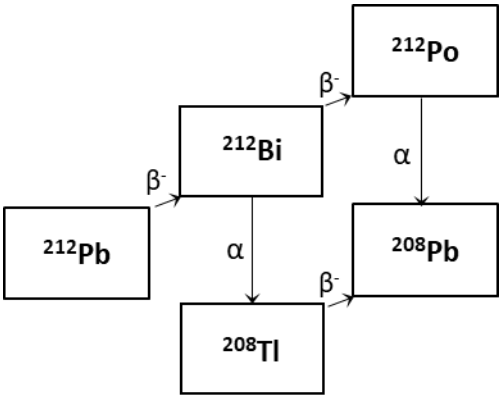

Figure 2 Normalized activity as a function of the triple-to-double coincidence ratio (*R*). Open circles are from Experiment 1; open triangles are from Experiment 2. The groupings reflect the application of different gray filters to vary the counting efficiency.

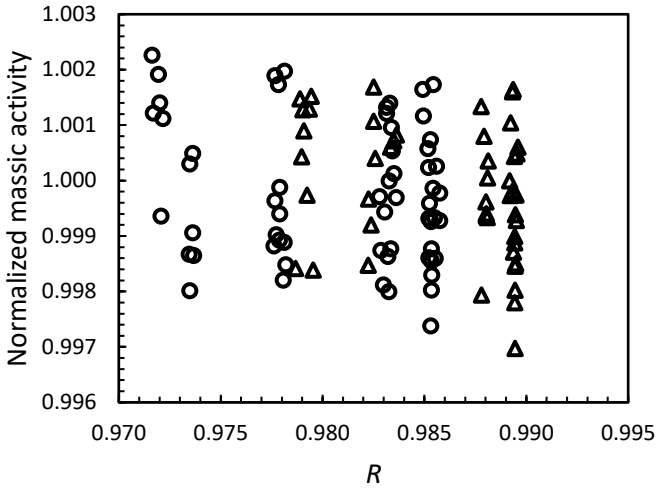

Figure 3 Normalized activity as a function of the ^{212}Pb efficiency in Experiment 1. Open circles reproduce the E1 TDCR data from Figure 2 where EFF(Pb-212) = ε_D; ×s represent CNET data acquired with the Beckman counter where EFF(Pb-212) is the traced efficiency; ∗s represent CNET data acquired with the TriCarb counter. The activities and efficiencies shown were calculated with the DDEP decay data; the results with the NNDC data were nearly identical. The MICELLE2 model describes the TDCR and CNET data consistently and without bias as a function of efficiency.

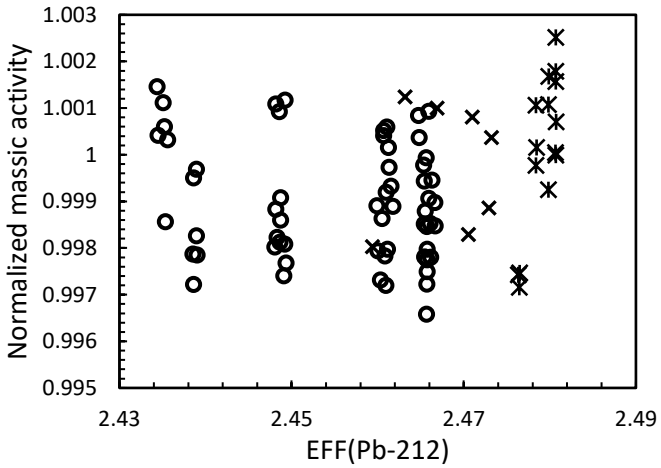

Figure 4 Geant4 NaI spectra for Pb-212 (solid black), Bi-212 with Po-212 (solid red) and Tl-208 (dashed blue). LTAC gates (dotted black boxes) from left to right: Gate 1, focused on Pb-212; gate 2, focused on Bi-212, and Gate 3 focused on Tl-208.

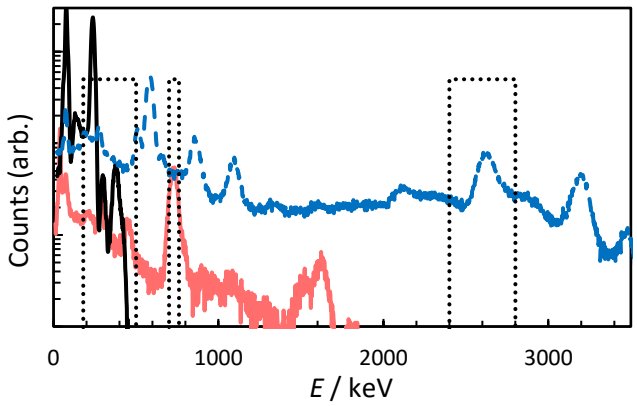

Figure 5 Representative experimental LTAC data for the effective gate $Y_{eff} = 0.20 \cdot Y_1 + 0.41 \cdot Y_2 + 0.39 \cdot Y_3$. The black dotted line shows a linear extrapolation that gives the LS count rate, R_{LS}, expected for perfect counting efficiency. Below, the relative fit residuals, r, are shown for the same experimental data (black circles) and for the GEANT4 model (open gray circles).

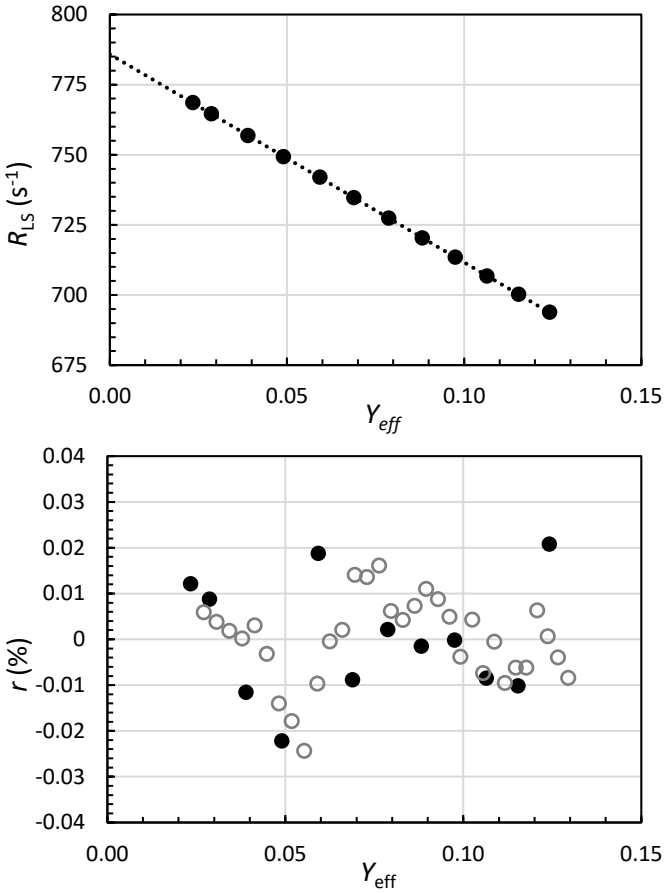

Figure S1 Experimental scheme showing the gravimetric dilutions carried out in both experiments.